

## Field-induced metamagnetic transitions and two-dimensional excitations in ludwigite $\text{Co}_{4.76}\text{Al}_{1.24}(\text{O}_2\text{BO}_3)_2$

C. P. C. Medrano,<sup>1</sup> D. C. Freitas,<sup>1,2</sup> E. C. Passamani,<sup>3</sup> C. B. Pinheiro,<sup>4</sup> E. Baggio-Saitovitch,<sup>2</sup> M. A. Continentino,<sup>2,\*</sup> and D. R. Sanchez<sup>1</sup>

<sup>1</sup>*Instituto de Física, Universidade Federal Fluminense, Campus da Praia Vermelha, 24210-346 Niterói, Rio de Janeiro, Brazil*

<sup>2</sup>*Centro Brasileiro de Pesquisas Físicas, Rua Doutor Xavier Sigaud, 150-Urca 22290-180 Rio de Janeiro, Rio de Janeiro, Brazil*

<sup>3</sup>*Departamento de Física, Universidade Federal do Espírito Santo, Vitória 29060-900, Espírito Santo, Brazil*

<sup>4</sup>*Departamento de Física, Instituto de Ciências Exatas, Universidade Federal de Minas Gerais, Campus da Pampulha, Caixa Postal 702, 30123-970 Belo Horizonte, Minas Gerais, Brazil*

(Received 25 January 2017; revised manuscript received 31 May 2017; published 26 June 2017)

This paper presents an extensive study of the structural, magnetic, and thermodynamic properties of the heterometallic ludwigite  $\text{Co}_{4.76}\text{Al}_{1.24}(\text{O}_2\text{BO}_3)_2$ . This material orders ferrimagnetically at 57 K. Despite the fact that, in  $\text{Co}_{4.76}\text{Al}_{1.24}(\text{O}_2\text{BO}_3)_2$ , one quarter of the Co ions of the parent compound  $\text{Co}_3\text{O}_2\text{BO}_3$  is replaced by nonmagnetic  $\text{Al}^{3+}$  ions, the  $T_C$  of the former (57 K) is larger than that of the latter (42 K). We obtain the phase diagram of  $\text{Co}_{4.76}\text{Al}_{1.24}(\text{O}_2\text{BO}_3)_2$  in an external magnetic field. We find a line of second-order phase transitions where the system presents a metamagnetic transition (from 57 to 25 K). This line ends at a tricritical point at 25 K and 4.3 T, below which the transition to the paramagnetic phase is first order (from 25 to 3 K). In the magnetic phase at low temperatures specific heat measurements in zero and finite magnetic fields show that the low-energy excitations are magnetic (magnons) and elastic (phonons) excitations with two-dimensional character. These measurements also reveal the magnetocaloric properties of this material.

DOI: [10.1103/PhysRevB.95.214419](https://doi.org/10.1103/PhysRevB.95.214419)

### I. INTRODUCTION

The ludwigites have the general chemical formula  $M_2^{2+}M'^{3+}\text{O}_2\text{BO}_3$  and crystallize in the orthorhombic structure space-group  $Pbam$  where the metals ( $M$  and  $M'$ ) occupy four nonequivalent crystallographic positions inside of oxygen octahedrons. The metals are arranged in such a way that form two subunits, so-called three leg ladders, assigning to the ludwigites a low-dimensional character. These compounds are divided in two subgroups, the homometallic ( $M = M'$ ) and the heterometallic ( $M \neq M'$ ) ludwigites [1]. Until now only two homometallic ludwigites were reported in the literature,  $\text{Fe}_3\text{O}_2\text{BO}_3$  [2–5] and  $\text{Co}_3\text{O}_2\text{BO}_3$  [6,7]. The former one is the most studied, and a wide variety of physical phenomena, such as partial magnetic order, charge ordering, and structural transitions, were observed for this compound [2–5].  $\text{Co}_3\text{O}_2\text{BO}_3$  seemed to be a simple compound showing only one magnetic transition of the whole system at 42 K without signs of charge ordering nor structural transition. However, recently, neutron studies revealed a coexistence of high spin (HS) and low spin (LS) states in one of the three legged ladders of this material, giving rise to new insights on the magnetic structure and the interactions involved in  $\text{Co}_3\text{O}_2\text{BO}_3$  [8].

Motivated by the unexpected differences between Co and Fe homometallic ludwigites, many other heterometallic ludwigites were synthesized [9–13]. The study of these latter compounds show that the magnetic interactions between different types of magnetic ions are more complex and lead to a spin-glass freezing or to a reduction of the effective magnetic moments [9–13].

With the aim of simplifying the magnetic complexity,  $\text{Co}_3\text{O}_2\text{BO}_3$  was diluted diamagnetically by substituting Co

with Ti [14], Mg [15], Ga [16], and Sn [17] ions. As shown in these works, nonmagnetic Ti, Mg, and Ga ions can reduce or even destroy long-range magnetic order. On the other hand, Sn drastically raised the magnetic ordering [17]. In ludwigites with  $\text{Co}^{2+}$  and  $\text{Co}^{3+}$  a strong competition between superexchange and double exchange interactions is expected. In  $\text{Co}_5\text{Sn}(\text{O}_2\text{BO}_3)_2$  [17] 50% of the ions at sites 4 are occupied by  $\text{Sn}^{4+}$ , which leads to all the Co ions to assume the valence state 2+. Then, the unexpected enhancement of the magnetism in  $\text{Co}_5\text{Sn}(\text{O}_2\text{BO}_3)_2$  was attributed to the absence of the double exchange interactions that reduce the magnetic frustration [17].

In this paper we study  $\text{Co}_{4.76}\text{Al}_{1.24}(\text{O}_2\text{BO}_3)_2$  in comparison with  $\text{Co}_3\text{O}_2\text{BO}_3$  and  $\text{Co}_5\text{Sn}(\text{O}_2\text{BO}_3)_2$ . The new heterometallic ludwigite  $\text{Co}_{4.76}\text{Al}_{1.24}(\text{O}_2\text{BO}_3)_2$  shows some properties never seen before in other ludwigites: Metamagnetic transitions with moderate applied magnetic fields of first and second order, the magnetocaloric effect, and the  $T^2$  dependence of the specific heat at low temperatures attributed to magnon and phonon planar excitations. In addition, an increase in the magnetic order temperature is observed as in  $\text{Co}_5\text{Sn}(\text{O}_2\text{BO}_3)_2$ . These results open the question about the role of the spin state of  $\text{Co}^{3+}$  in these kinds of compounds.

### II. EXPERIMENT

#### A. Synthesis

The crystals were synthesized from a 5:1:2 molar mixture of  $\text{Co}_3\text{O}_4:\text{Al}_2\text{O}_3:\text{H}_3\text{BO}_3$  with an excess of borax in an aluminum crucible. The mixture was heated at 1160 °C for 24 h and cooled down to 600 °C for 48 h. Then the oven was turned off. The bath was dissolved in hot water and the crystals washed in diluted hydrochloric acid. Needle-shaped black crystals up to 5 mm in length were obtained. The purity of the sample was confirmed by x-ray powder and single-crystal diffractions.

\*mucio@cbpf.br

### B. Structural characterization

Single-crystal x-ray-diffraction data collections were performed using a sealed tube Oxford-Diffraction GEMINI diffractometer. Measurements were performed at 270 and 120 K. The x-ray-diffraction data integration and scaling of reflection intensities were performed with the CRYSTALIS *suite* [18]. Final unit-cell parameters were based on fitting of all measured reflection positions. Analytical [19] and semiempirical [20] absorption corrections were performed using the CRYSTALIS *suite* [18]. The program XPREP [21] was used for the space-group identification and final data reduction. The structures of all compounds were solved by direct methods using the SIR92 [22] program. The positions of all atoms could be assigned unambiguously on consecutive difference Fourier maps. Refinements were performed using SHELXL2013 [23] based on  $F^2$  through full-matrix least-squares routines. During the refinements substitutional disorder between cobalt and aluminum atoms was identified for sites with Wyckoff letters (see Table II)  $a$ ,  $d$ , and  $h$  of the space-group  $Pbam$  and refined with constrained parameters. All attempts to refine the disordered cobalt and aluminum atoms with independent atomic displacement parameters failed. After refinement, the atoms' content in a unit formula is  $\text{Co}_{9.51}\text{Al}_{2.49}(\text{O}_2\text{BO}_3)_4$ , which can be reduced to  $\text{Co}_{4.76}\text{Al}_{1.24}(\text{O}_2\text{BO}_3)_2$ . The structure was solved in analogous experimental conditions at 270 K and 120 K in order to observe any eventual change with temperature, and no evidence for any phase transition was found in this temperature range. Crystal data, data collection parameters, and structure refinement data for the measurement performed at 120 K are summarized in Table I.

Figure 1 on the left shows a schematic structure of  $\text{Co}_{4.76}\text{Al}_{1.24}(\text{O}_2\text{BO}_3)_2$  projected along the  $c$  axis; on the right, layers formed by sites 1, 2, and 3 parallel to the  $b$ - $c$  plane are shown in detail. The triangular coordination of site 2 on these layers is worth noting. These layers are 4.6 Å apart along the  $a$  axis.

Table II shows the fractional coordinates, the site occupation (Occ.), and equivalent isotropic displacement parameters. Site 3 is occupied exclusively by Co atoms. Sites 1, 2, and 4 are occupied randomly by Al and Co ions. The oxygen atoms on sites O4 and O2, which are not bonded to boron showed unusual large atomic displacement parameters. This particular feature could suggest a modulated structure as a function of the Co/Al substitution ratio whose occurrence is being investigated and will be published elsewhere. Oxidation numbers calculated with the bond valence sum method given by Wood and Palenik [24] ascribe valence 2+ for Co ions in sites 1 and 3 as occurs in most of the ludwigites. It should be noted that in these two sites no (or only a small fraction of) Al is found. As expected, an average valence (between +2 and +3) was obtained for Co at sites 2 and 4 if we consider that Al is positioned mainly at these two sites. The structural characteristics of this compound could be related to the proximity of the effective ionic radii of Al (0.535 Å) to that of LS  $\text{Co}^{3+}$  (0.545 Å). Just for comparison, the effective ionic radii of the HS  $\text{Co}^{3+}$  (0.61 Å) is larger and could be absent in this compound.

### C. Magnetic measurements

The dc magnetization measurements of  $\text{Co}_{4.76}\text{Al}_{1.24}(\text{O}_2\text{BO}_3)_2$  were performed on both powder and oriented

TABLE I. Crystal data and structure refinement of  $\text{Co}_{4.76}\text{Al}_{1.24}(\text{O}_2\text{BO}_3)_2$ .

Empirical formula from x-ray analysis	$\text{Co}_{4.76}\text{Al}_{1.24}\text{B}_2\text{O}_{10}$
Formula weight	495.42 g/mol
Wavelength	0.71073 Å
Crystal size	$0.145 \times 0.075 \times 0.050$ mm <sup>3</sup>
Temperature	120(2) K
Crystal system	Orthorhombic
Space group	(No. 55) $Pbam$
Unit-cell dimension $a =$	9.2048(2) Å
$b =$	12.0562(2) Å
$c =$	3.00070(10) Å
Volume	333.002(14) Å <sup>3</sup>
$Z$	2
Density (calculated)	4.941 Mg/m <sup>3</sup>
Absorption coefficient	11.826/mm
Absorption correction type	Analytical
$F(000)$	469
$\theta$ range (deg)	2.784–37.812
Index range $h =$	–15, 15
$k =$	–20, 20
$l =$	–5, 5
Reflections collected	38035
Independent reflections	1008
$R$ (int)	0.0720
Completeness to $\theta = 25.242$	100.0%
Refinement method: Full-matrix least squares on $F^2$	
data/restraints/parameters	1008/0/63
Goodness of fit on $F^2$	1.344
Final $R$ indices [ $I > 2\sigma(I)$ ]	$R1 = 0.0250, wR2 = 0.0646$
$R$ indices (all data)	$R1 = 0.0300, wR2 = 0.0666$
Extinction coefficient	0.0190(16)
Largest diff. peak	$0.837 e \text{ \AA}^{-3}$
Largest diff. hole	$-1.018 e \text{ \AA}^{-3}$

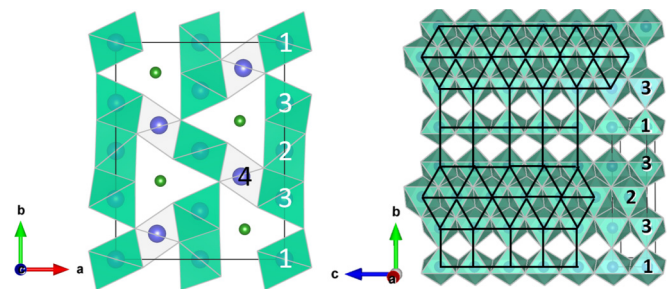


FIG. 1. On the left, a schematic structure of the unit cell of the ludwigites projected along the  $c$  axis is shown. The oxygen polyhedra centered on the metal ions are shown. The numbers indicate nonequivalent crystallographic metallic sites given in Table II. Boron ions (green spheres) have trigonal coordination. The projections of the layers formed by sites 1, 2, and 3 are emphasized in green. On the right is shown a different view of the plane formed by metal at sites 1, 2, and 3. Here we can see that there is a triangular coordination for metal site 2. These figures were generated by the VESTA 3.1.1 software [25].

TABLE II. Fractional coordinates, occupation, and equivalent isotropic displacement parameters ( $\text{\AA}^2 \times 10^3$ ) for  $\text{Co}_{4.76}\text{Al}_{1.24}(\text{O}_2\text{BO}_3)_2$ . The Occ. is the occupation of atoms per site, normalized by the site occupancy factor.  $U(\text{eq})$  is defined as one third of the trace of the orthogonalized  $U_{ij}$  tensor [26].

Site	$x/a$	$y/b$	$z/c$	Occ.	$U(\text{eq})$
Co1(2a)	0	0	0	0.882	4(1)
Al1(2a)	0	0	0	0.118	4(1)
Co2(2d)	0	0.5	-0.5	0.672	5(1)
Al2(2d)	0	0.5	-0.5	0.328	5(1)
Co3(4g)	-0.0020(1)	0.2787(1)	0	1	4(1)
Co4(4h)	0.2378(4)	0.1116(2)	-0.5	0.601	4(1)
Al4(4h)	0.2398(16)	0.1218(9)	-0.5	0.399	4(1)
B	0.2703(3)	0.3620(2)	-0.5	1	5(1)
O1	0.1516(2)	-0.0409(1)	-0.5	1	8(1)
O2	0.1101(2)	0.1419(1)	0	1	10(1)
O3	0.1204(2)	0.3631(1)	-0.5	1	7(1)
O4	-0.1155(2)	0.4262(1)	0	1	18(1)
O5	-0.1584(2)	0.2393(1)	-0.5	1	7(1)

single crystals using a commercial Quantum Design physical property measurement system.

Figure 2 shows the temperature dependence of the dc magnetization for FC and ZFC procedures for the applied field of 100 Oe. Cooling down, the magnetization increases progressively achieving a maximum value of  $6.6 \times 10^{-3} \mu_B/\text{f.u.}$ , which corresponds to the susceptibility value of  $8 \times 10^{-4} \text{ emu g}^{-1} \text{Oe}^{-1}$  at 57 K and decreases for lower temperatures. It must be pointed out the low values of the susceptibility for this compound when compared to those corresponding to  $\text{Co}_3\text{O}_2\text{B}_2\text{O}_3$  ( $\sim 2 \times 10^{-2} \text{ emu g}^{-1} \text{Oe}^{-1}$  at 42 K [6]), which are two orders of magnitude larger. The paramagnetic region above 180 K follows the Curie-Weiss

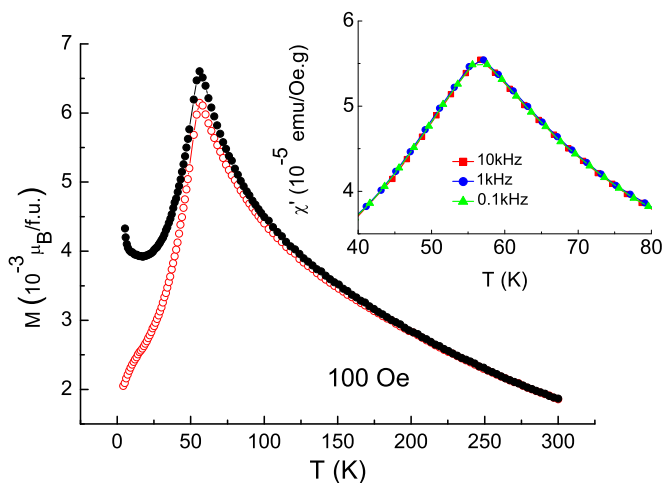


FIG. 2. Magnetization versus temperature for  $\text{Co}_{4.76}\text{Al}_{1.24}(\text{O}_2\text{BO}_3)_2$  under an applied magnetic field of 100 Oe in both regimes: field-cooled [(FC): closed symbol] and zero-field-cooled [(ZFC): open symbol]. The inset shows the real part ( $\chi'$ ) of the ac magnetic susceptibility of  $\text{Co}_{4.76}\text{Al}_{1.24}(\text{O}_2\text{BO}_3)_2$  as functions of temperature for 100 Hz, 1, and 10 kHz close to the region of the peak.

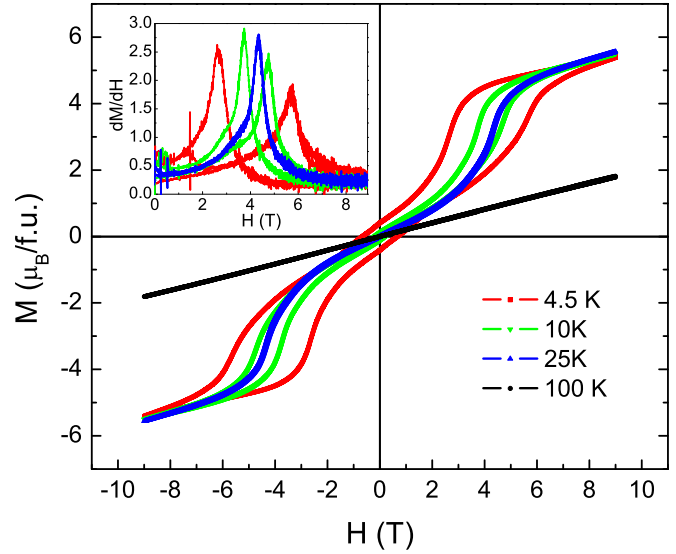


FIG. 3.  $\text{Co}_{4.76}\text{Al}_{1.24}(\text{O}_2\text{BO}_3)_2$  magnetization versus applied magnetic-field curves at 4.5, 10, 25, and 100 K. The inset shows the derivative of the curves.

law with  $C = 31.37 \times 10^{-3} \text{ emu K g}^{-1} \text{Oe}^{-1}$  and Curie-Weiss temperature of  $\theta_{CW} = -4.81 \text{ K}$ . The small  $|\theta_{CW}|/T_C$  ratio indicates competing ferromagnetic (FM) and antiferromagnetic interactions at high temperatures. From the Curie constant we determine the effective moment per unit formula  $p_{\text{eff}} = 11.24 \mu_B$ . The charge balance on  $\text{Co}_{4.76}\text{Al}_{1.24}(\text{O}_2\text{BO}_3)_2$  leaves four atoms of  $\text{Co}^{2+}$  and 0.76 atoms of  $\text{Co}^{3+}$  per unit formula. If all the atoms are in the HS state, the spin only moment gives  $p = \sqrt{4(3.87)^2 + 0.76(4.90)^2} = 8.84 \mu_B$ . A configuration with  $\text{Co}^{2+}$  in the HS state and  $\text{Co}^{3+}$  in the LS state ( $S = 0$ ) gives  $p = 7.74 \mu_B$  (in both cases  $g = 2$  was considered). Then, in any case, there is a reasonable orbital contribution to the total magnetic moment, characteristic of  $\text{Co}^{2+}$  magnetic ions as observed previously in  $\text{Co}_3\text{O}_2\text{BO}_3$  [8] and  $\text{Co}_5\text{Sn}(\text{O}_2\text{BO}_3)_2$  [17]. Figure 2 shows ac-susceptibility measurements for different frequencies as a function of temperature. A peak is observed at 57 K whose position does not change with frequency (see the inset), characteristic of a long-range magnetic ordering.

The magnetization curves as a function of applied magnetic fields for different temperatures are shown in Fig. 3. At 100 K the magnetization exhibits a paramagnetic behavior, i.e., it increases linearly with the applied magnetic field. For fixed temperatures below  $T_C$ , the magnetization presents an inflection point at a critical field  $H_c$ , compatible with a metamagnetic transition. This is seen better in the inset of Fig. 3 where it appears as a maximum in the derivative  $\partial M/\partial H$ .

Figure 4 shows magnetization measurements in oriented single crystals with the applied magnetic field along and perpendicular to the  $c$  axis. The results are compatible with a highly anisotropic compound with the easy magnetization direction on the  $a$ - $b$  plane. A small remanent magnetization ( $\sim 0.1 \mu_B/\text{f.u.}$ ) is observed in the hysteresis curves taken with the applied field perpendicular to the  $c$  axis (see the inset of Fig. 4).

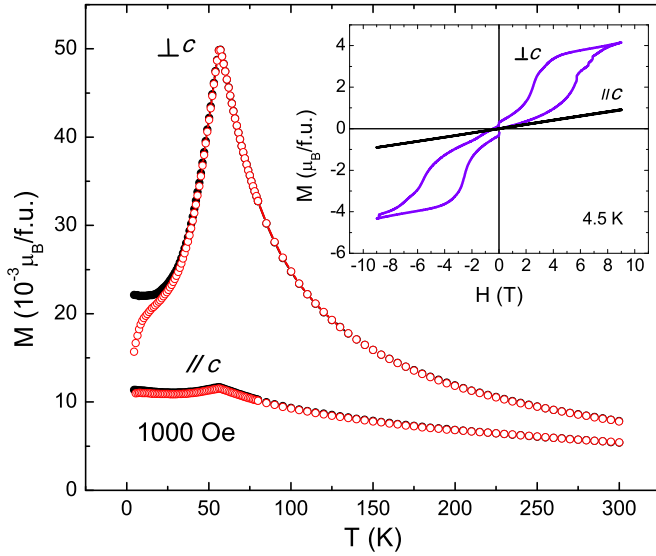


FIG. 4.  $\text{Co}_{4.76}\text{Al}_{1.24}(\text{O}_2\text{BO}_3)_2$  magnetization versus temperature under an applied field of 1000 Oe in both regimes: field cooled (FC: closed symbol) and zero-field cooled (ZFC: open symbol) for oriented crystals. The inset shows the hysteresis loops for oriented crystals at 4.5 K.

#### D. Specific heat measurements

Specific heat measurements as a function of temperature and magnetic field were performed in 3 mg of randomly oriented crystalline needles.

Figure 5 shows specific heat curves plotted as  $C/T$  versus  $T$  for  $\text{Co}_{4.76}\text{Al}_{1.24}(\text{O}_2\text{BO}_3)_2$  in applied magnetic fields of 0, 3, 5, and 9 T. The specific heat at 0 T has a peak at  $T_C = 57$  K that shifts to lower temperatures with increasing applied magnetic field and eventually disappears. The inset of Fig. 5 shows the plot of  $C/T^2$  versus  $T$  for zero- and 9-T applied magnetic

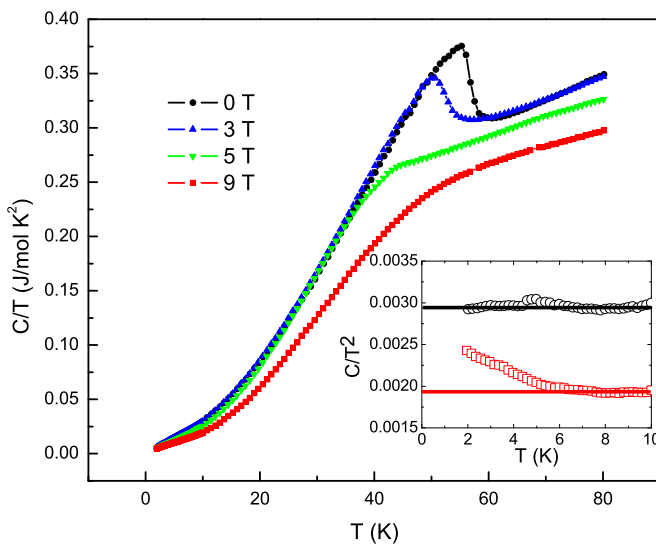


FIG. 5.  $\text{Co}_{4.76}\text{Al}_{1.24}(\text{O}_2\text{BO}_3)_2$  specific heat plotted as  $C/T$  versus  $T$  for applied magnetic fields of 0, 3, 5, and 9 T. The inset: Low-temperature specific heat versus temperature for 0 and 9 T. The lines through the data are fittings to a power-law  $C = aT^2$  (see the text).

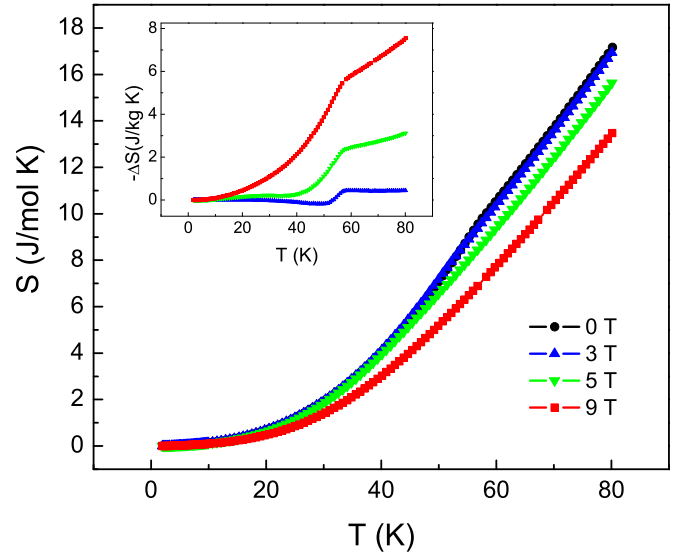


FIG. 6. Entropy as a function of temperature obtained from the specific heat curves for  $\text{Co}_{4.76}\text{Al}_{1.24}(\text{O}_2\text{BO}_3)_2$  at applied fields of 0, 3, 5, and 9 T. The inset: Isothermal magnetic entropy change  $[-\Delta S = S(H = 0) - S(H \neq 0)]$  of  $\text{Co}_{4.76}\text{Al}_{1.24}(\text{O}_2\text{BO}_3)_2$  as a function of temperature for magnetic-field changes up to 9 T.

fields. For the zero field a  $T^2$  power law describes the low-temperature data well. The 9-T field besides reducing the low-temperature specific heat modifies its temperature dependence, although at higher temperatures a  $T^2$  power law describes well the data again. We postpone a detailed discussion of these results to Sec. III. However, it is evident from the data that the low-temperature specific heat in the zero field is dominated by magnetic excitations that are quenched by the large magnetic field.

Figure 6 shows the entropy as a function of temperature obtained from the specific heat curves (Fig. 5). Notice that between 23 and 54 K the curve for the 3-T magnetic field presents what is called the *inverse magnetocaloric effect* since the entropy at this field is larger than that in the zero field. Similar behaviors have been observed in other ferrimagnetic systems at low temperatures and applied magnetic fields [27,28]. The sensitivity of the variation in magnetic entropy as a function of temperature for different magnetic fields ( $-\Delta S = 7.5 \text{ J kg}^{-1} \text{ K}^{-1}$  at 80 K for  $\Delta H = 9$ ) makes this compound likely to be applied in magnetic refrigeration.

### III. DISCUSSION

In  $\text{Co}_3\text{O}_2\text{BO}_3$  ions with charge 3+ occupy sites 4 leaving sites 1, 2, and 3 to be occupied by ions with charge 2+ [6]. Single-crystal x-ray experiments in  $\text{Co}_{4.76}\text{Al}_{1.24}(\text{O}_2\text{BO}_3)_2$  have shown that  $\text{Al}^{3+}$  enters mainly in site 4 and in a minor proportion in sites 2 and 1 (see Table II). Here it is important to point out that the presence of  $\text{Al}^{3+}$  at different sites in  $\text{Co}_{4.76}\text{Al}_{1.24}(\text{O}_2\text{BO}_3)_2$  forces a fraction of Co ions at site 4 (at least  $\sim 20\%$ ) to adopt the valence 2+.

Comparing the results for  $\text{Co}_3\text{O}_2\text{B}_2\text{O}_3$  [6] and  $\text{Co}_5\text{Sn}(\text{O}_2\text{BO}_3)_2$  [17] seems to imply a direct relation between the  $T_C$  and the amount of  $\text{Co}^{2+}$  ions in site

4:  $T_C = 42$  K for 0% in  $\text{Co}_3\text{O}_2\text{B}_2\text{O}_3$  [6],  $T_C = 57$  K for  $\sim 20\%$  in  $\text{Co}_{4.76}\text{Al}_{1.24}(\text{O}_2\text{BO}_3)_2$ , and  $T_C = 82$  K for 50% in  $\text{Co}_5\text{Sn}(\text{O}_2\text{BO}_3)_2$  [17]. The Curie-Weiss temperature is small compared to  $T_C$  indicating competition between interactions with different signs and that frustration is important in this system. Below  $T_C$  the magnetization measurements of oriented crystals indicate that the  $c$  axis is a hard magnetization direction as happens in  $\text{Co}_3\text{O}_2\text{B}_2\text{O}_3$ .

The hysteresis loops (Fig. 3) shows a small remanent magnetization below  $T_C$  indicating a ferrimagnetic (FIM) structure in agreement with the specific heat results (see the discussion below). Below the magnetic transition the sigmoidal shapes of the magnetic hysteresis loop are unusual for ludwigites. These curves have inflection points better seen as maxima in the derivatives. The field and the temperature at which it occurs define a metamagnetic transition line at  $T_c(H_c)$  in  $\text{Co}_{4.76}\text{Al}_{1.24}(\text{O}_2\text{BO}_3)_2$  ludwigite. As temperature is further reduced, the  $M(H)$  curves become hysteretic down to the lowest temperatures as can be seen in Fig. 3. The appearance of hysteresis for  $T < T_t$  and  $H > H_t$  sets the existence of a tricritical point at  $(T_t$  and  $H_t)$  in the  $T_c(H_c)$  phase diagram (Fig. 7) such that for  $T < T_t$  and  $H > H_t$  the ferrimagnetic-paramagnetic transition becomes first order. The two maxima on the  $\partial M/\partial H$  curves point the limits of stability of these different phases coexisting at the first-order line. The phase diagram obtained from the  $\chi'(T)$ ,  $C(T,H)$ , and  $M(T,H)$  measurements is presented in Fig. 7. This metamagnetic transition is related to magnetic ions in a frustrated state, which are flipped at moderate critical fields increasing the magnetization abruptly.

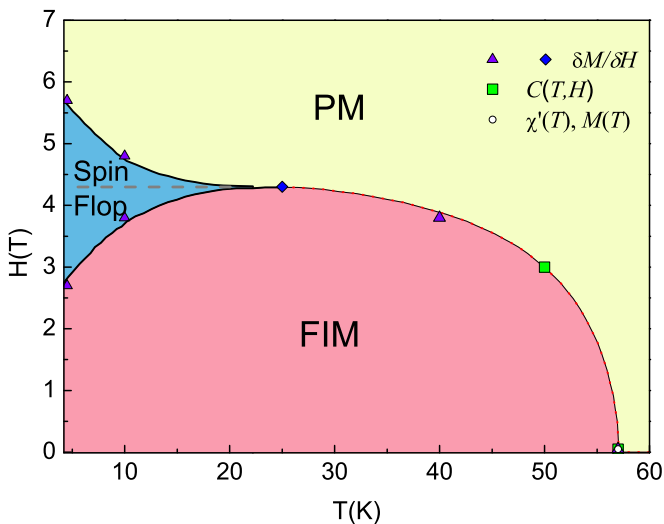


FIG. 7. The phase diagram of  $\text{Co}_{4.76}\text{Al}_{1.24}(\text{O}_2\text{BO}_3)_2$ . The phase boundaries were determined as follows: The white circle is the transition temperature obtained from the magnetic susceptibility  $\chi(T)$  and magnetization  $M(T)$ . The green squares are from specific heat  $C(T,H)$ , and the purple triangles are from  $\partial M/\partial H$ . Three phases are defined as follows: paramagnetic (PM), FIM, and spin flop. A tricritical point separating the lines of second- and first-order transitions appears at  $(H_t = 4.2$  T,  $T_t = 25$  K), indicated by a blue diamond symbol. The *spin-flop* phases are in fact metastable phases where FIM and PM phases coexist.

Specific heat results indicate ferrimagnetic ordering as the peak is not suppressed but shifts to lower temperatures with increasing magnetic field. This behavior is novel in Co ludwigites. For sufficiently strong magnetic fields there is no sign of FIM transitions in agreement with the magnetic phase diagram shown in Fig. 7. The low-temperature specific heat shows a dominant  $T^2$  contribution in a zero field. This contribution arises due to gapless excitations with a linear dispersion relation  $\hbar\omega = vk$  in two-dimensional (2D) systems. A straightforward calculation in this case yields  $C = 14.4R(T/T^*)^2 = aT^2$  ( $\text{J mol}^{-1} \text{K}^{-1}$ ) where  $R$  is the universal gas constant and the characteristic temperature  $T^*$  is related to a cutoff wave-vector  $k_c$  by  $k_B T^* = vk_c$ . In a magnetic field of 9 T and for low temperatures these excitations are quenched, and the specific heat is reduced. The low-temperature behavior deviates from the  $T^2$  behavior due to a Zeeman gap in the spectrum of magnetic excitations as shown in the inset of Fig. 5. In this case, we attribute the low-temperature specific heat entirely to the excitation of 2D acoustic phonons with linear dispersion. Using the coefficient of the  $T^2$  term of the 9-T specific heat obtained from the inset of Fig. 5,  $a(9 \text{ T}) = 0.00194 \text{ J mol}^{-1} \text{K}^{-3}$ , we obtain for the elastic characteristic temperature  $T_E^* = 252$  K. This is on the order of magnitude of the Debye temperature obtained for other ludwigites [6,9,14,17]. In the zero field it is natural to assume that the  $T^2$  term arises due to the contribution of both, 2D phonons and 2D FIM magnons with linear dispersion. Since the experiments yield  $a(0 \text{ T}) = 0.00295 \text{ J mol}^{-1} \text{K}^{-3}$ , we obtain  $T_M^* = 335$  K where we used  $T_E^* = 252$  K. This is to be compared with the Curie-Weiss temperature or the magnetic ordering temperature. Then, our assumption that the low-temperature specific heat of the  $\text{Co}_{4.76}\text{Al}_{1.24}(\text{O}_2\text{BO}_3)_2$  ludwigite is due to linear dispersing elastic and magnetic excitations on planes gives a tentative approximation for the description of the thermodynamic properties of this system at low  $T$ . It is interesting that, from the point of view of the elastic properties, the present system also presents two-dimensional character. This  $T^2$  contribution also was observed in two-dimensional compounds as in the hulsite  $\text{Co}_5\text{Sb}(\text{O}_2\text{BO}_3)_2$  formed by two families of parallel sheets [29].

A possible scenario for the magnetic structure of  $\text{Co}_{4.76}\text{Al}_{1.24}(\text{O}_2\text{BO}_3)_2$ , compatible with the two-dimensional character, is to consider magnetic planes composed by  $\text{Co}^{2+}$  in sites 1,2, and 3 (1-2-3 planes) separated by nonmagnetic ions ( $\text{Al}^{3+}$  and LS  $\text{Co}^{3+}$ ) at sites 4 as occur in  $\text{Co}_3\text{O}_2\text{B}_2\text{O}_3$  [6] where site 4 is occupied by a LS  $\text{Co}^{3+}$  (see Fig. 1). This scenario is compatible with frustration of the magnetic ions [30] at sites 2 due to a planar triangular coordination and that is reduced by the presence of nonmagnetic Al ions in this site. As a consequence of the softly frustrated site 2, metamagnetic transition could take place. Further studies are in progress to confirm such a hypothesis. So, the knowledge of the real state spin of  $\text{Co}^{3+}$  seems to be the key to answer to questions about the magnetic structure and the properties shown by this and related compounds.

The observation of the negative magnetocaloric effect is associated with the system crossing the field-dependent critical line. Above 3 T all the magnetic moments are aligned along the magnetic field (see the phase diagram Fig. 7) and as expected

for a FM system the entropy change  $-\Delta S$  takes positive values [27,28].

In conclusion, in the  $\text{Co}_{4.76}\text{Al}_{1.24}(\text{O}_2\text{BO}_3)_2$  ludwigite a long-range magnetic order of the whole compound is observed below 57 K. This temperature is higher than that of the homometallic  $\text{Co}_3\text{O}_2\text{BO}_3$  (42 K) but lower than that of  $\text{Co}_5\text{Sn}(\text{O}_2\text{BO}_3)_2$  (82 K). Like in  $\text{Co}_5\text{Sn}(\text{O}_2\text{BO}_3)_2$ , the magnetic transition temperature is raised by the presence of nonmagnetic ions. Magnetic and thermal results for  $\text{Co}_{4.76}\text{Al}_{1.24}(\text{O}_2\text{BO}_3)_2$  indicate a ferrimagnetic order. Magnetic measurements under applied magnetic fields revealed the presence of magnetically frustrated spins leading to metamagnetic transitions. The critical field at which the metamagnetic transitions occur is temperature dependent, and a magnetic

phase diagram can be constructed showing three regions, PM, FIM, and spin-flop phases with first- and second-order transitions among them. Heat-capacity measurements show magnetocaloric effects and at low temperatures show  $T^2$  dependences that could be related to two-dimensional character. Such properties have not been observed in ludwigites so far.

#### ACKNOWLEDGMENTS

Support from the Brazilian agencies CNPq and FAPERJ is gratefully acknowledged. We also acknowledge LDRX-UFF (Universidade Federal Fluminense, Brazil) for use of their laboratory facilities.

- 
- [1] M. A. Continentino, J. C. Fernandes, R. B. Guimarães, B. Boechat, and A. Saguia, in *Frontiers in Magnetic Materials*, edited by A. V. Narlikar (Springer, Berlin, 2005), pp. 385–410.
- [2] M. Mir, R. B. Guimarães, J. C. Fernandes, M. A. Continentino, A. C. Doriguetto, Y. P. Mascarenhas, J. Ellena, E. E. Castellano, R. S. Freitas, and L. Ghivelder, *Phys. Rev. Lett.* **87**, 147201 (2001).
- [3] P. Bordet and E. Suard, *Phys. Rev. B* **79**, 144408 (2009).
- [4] R. B. Guimarães, M. Mir, J. C. Fernandes, M. A. Continentino, H. A. Borges, G. Cernicchiaro, M. B. Fontes, D. R. S. Candela, and E. Baggio-Saitovitch, *Phys. Rev. B* **60**, 6617 (1999).
- [5] J. C. Fernandes, R. B. Guimarães, M. A. Continentino, L. Ghivelder, and R. S. Freitas, *Phys. Rev. B* **61**, R850 (2000).
- [6] D. C. Freitas, M. A. Continentino, R. B. Guimarães, J. C. Fernandes, J. Ellena, and L. Ghivelder, *Phys. Rev. B* **77**, 184422 (2008).
- [7] N. B. Ivanova, A. D. Vasiliev, D. A. Velikanov, N. V. Kazak, S. G. Ovchinnikov, G. A. Petrakovskii, and V. V. Rudenko, *Phys. Solid State* **49**, 651 (2007).
- [8] D. C. Freitas, C. P. C. Medrano, D. R. Sanchez, M. N. Regueiro, J. A. Rodríguez-Velamazán, and M. A. Continentino, *Phys. Rev. B* **94**, 174409 (2016).
- [9] D. C. Freitas, M. A. Continentino, R. B. Guimarães, J. C. Fernandes, E. P. Oliveira, R. E. Santelli, J. Ellena, G. G. Eslava, and L. Ghivelder, *Phys. Rev. B* **79**, 134437 (2009).
- [10] J. Bartolomé, A. Arauzo, N. V. Kazak, N. B. Ivanova, S. G. Ovchinnikov, Y. V. Knyazev, and I. S. Lyubutin, *Phys. Rev. B* **83**, 144426 (2011).
- [11] N. B. Ivanova, N. V. Kazak, Y. V. Knyazeva, D. A. Velikanova, L. N. Bezmaternykh, S. G. Ovchinnikova, A. D. Vasiliev, M. S. Platunov, J. Bartolomé, and G. S. Patrino, *J. Exp. Theor. Phys.* **113**, 1015 (2011).
- [12] Y. V. Knyazev, N. B. Ivanova, N. V. Kazak, M. S. Platunov, L. N. Bezmaternykh, D. A. Velikanov, A. D. Vasiliev, S. G. Ovchinnikov, and G. Yu Yurkin, *J. Magn. Magn. Mater.* **324**, 923 (2012).
- [13] N. V. Kazak, N. B. Ivanova, O. A. Bayukov, S. G. Ovchinnikov, A. Vasiliev, V. V. Rudenko, J. Bartolomé, A. Arauzo, and Y. V. Knyazev, *J. Magn. Magn. Mater.* **323**, 521 (2011).
- [14] D. C. Freitas, R. B. Guimarães, D. R. Sanchez, J. C. Fernandes, M. A. Continentino, J. Ellena, A. Kitada, H. Kageyama, A. Matsuo, K. Kindo, G. G. Eslava, and L. Ghivelder, *Phys. Rev. B* **81**, 024432 (2010).
- [15] N. B. Ivanova, M. S. Platunov, Y. V. Knyazev, N. V. Kazak, L. N. Bezmaternykh, E. V. Eremin, and A. D. Vasiliev, *Low Temp. Phys.* **38**, 172 (2012).
- [16] N. B. Ivanova, M. S. Platunov, Y. V. Knyazev, N. V. Kazak, L. N. Bezmaternykh, E. V. Eremin, and A. D. Vasiliev, *Phys. Solid State* **54**, 2212 (2012).
- [17] C. P. C. Medrano, D. C. Freitas, D. R. Sanchez, C. B. Pinheiro, G. G. Eslava, L. Ghivelder, and M. A. Continentino, *Phys. Rev. B* **91**, 054402 (2015).
- [18] Agilent Technologies CRYSLIS Pro (Agilent Technologies Ltd., Yarnton, UK, 2011).
- [19] R. C. Clark and J. S. Reid, *Acta Crystallogr. A* **51**, 887 (1995).
- [20] Empirical absorption correction using spherical harmonics, implemented in the SCALE3 ABSPACK scaling algorithm.
- [21] G. M. Sheldrick, XPREP (Bruker-AXS, Madison, WI, 2001).
- [22] A. Altomare, G. Cascarano, C. Giacovazzo, A. Guagliardi, M. C. Burla, G. Polidori, and M. Camalli, *J. Appl. Crystallogr.* **27**, 435 (1994).
- [23] G. M. Sheldrick, *Acta Crystallogr. A* **64**, 112 (2008).
- [24] R. M. Wood and G. J. Palenik, *Inorg. Chem.* **37**, 4149 (1998); D. C. de Freitas, M.Sc. thesis, Universidade Federal Fluminense, 2007.
- [25] K. Momma and F. Izumi, *J. Appl. Crystallogr.* **44**, 1272 (2011).
- [26] *International Tables for Crystallography*, 5th ed., edited by T. Hahn (Springer, Dordrecht, 2005), Vol. A, p. 283.
- [27] T. Samantaa, I. Das, and S. Banerjee, *Appl. Phys. Lett.* **91**, 152506 (2007).
- [28] R. D. dos Reis, L. M. da Silva, A. O. dos Santos, A. M. N. Medina, L. P. Cardoso, and F. C. G. Gandra, *J. Alloys Compd.* **582**, 5 (2014).
- [29] D. C. Freitas, R. B. Guimarães, J. C. Fernandes, M. A. Continentino, C. B. Pinheiro, J. A. L. C. Resende, G. G. Eslava, and L. Ghivelder, *Phys. Rev. B* **81**, 174403 (2010).
- [30] N. Tristan, V. Zestrea, G. Behr, R. Klingeler, B. Büchner, H. A. K. von Nidda, A. Loidl, and V. Tsurkan, *Phys. Rev. B* **77**, 094412 (2008).